The Generalized-Line-Based Iterative Transformation Model for Imagery Registration and Rectification

Chang Li and Wenzhong Shi

***Abstract*—Imagery registration and rectification is a process of transforming different sets of data into one coordinate system. A new model, i.e., the generalized-line-based iterative transformation model (GLBITM), is proposed by integrating the line-based transformation model (LBTM) and generalized point photogrammetry (GPP). First, the initial value of an affine transformation is acquired by LBTM. Then, on the basis of ground control lines (GCLs), not ground control points, the linear feature adjustment model with GPP is extended to a quadratic polynomial model and utilized to iteratively solve transformation coefficients. This process eliminates the translation amount and recalculates the scale and rotation coefficients. The authors suggest an iterative method with variable weights that is based on posterior variance estimation to improve quality control. A significant characteristic of the GLBITM is that the two endpoints of the corresponding GCLs are not necessarily conjugate points. The GLBITM integrates the advantages of the LBTM and GPP and avoids their respective shortfalls. Finally, this experiment verifies that the GLBITM gives correct, robust, and effective results that can be applied in high-resolution satellite imagery processing of multiple sensors, angles, and resolutions.**

***Index Terms*—Generalized-line-based iterative transformation model (GLBITM), ground control lines (GCLs), imagery registration, iterative method with variable weights, polynomial model, posterior variance estimation.**

I. Introduction

IMAGE-to-image registration is widely used in many disciplines, including computer vision, medical imaging, military automatic target recognition, and compiling and analyzing satellite images and data. Images may consist of multiple photographs, produced by different sensors, at different times and viewpoints. Several approaches have been proposed for image-to-image registration [1]–[4]. These transformation models are based on control points. In some remote areas, there may be lack of such control points. However, other image features (e.g., linear features) may be available. In fact, linear features add more information, increase redundancy, and improve the geometric strength of adjustment [5]. Linear features also have higher semantic information than point features and are easier to detect and digitize than point features [6]. Moreover, corresponding ground space lines can be identified from digital maps, Geographic Information System layers, or by Global Positioning System surveying techniques. Therefore, making use of linear features for image registration and rectification has more theoretical significance than traditional methods based on point features.

Based on the modified iterative Hough transform, Habib and Alruzouq established a new approach for automatic image registration with line segment endpoints [7]. It was noted that this proposed approach works well only if the transformation function is valid. Shi and Shaker presented a novel model [the line-based transformation model (LBTM)] for image-to-image registration [6], but this method is not a pure line-based transformation; it needs a ground control point (GCP) to recalculate the translation coefficients. An important motivation for this work is to address how to solve the affine transformation problem using only ground control lines (GCLs) and not GCPs. Generalized point photogrammetry (GPP) [8]–[10] includes physical point, feature line point, and the invisible point—infinity (vanishing point) into adjustment model—collinear equations. However, GPP cannot solve the problem of autoacquiring the initial approximation values for adjustment. Therefore, to integrate the advantages of both LBTM and GPP, a new model needs to be developed.

In this letter, a generalized-line-based iterative transformation model (GLBITM) is presented, which utilizes GCLs without any GCPs and obtains reliable and accurate results by using an iteration method with variable weights. Details of the approach are introduced and discussed in the following sections.

II. Methodology

The logic flow for the authors' approach of image-to-image registration and rectification is depicted in Fig. 1. The GLBITM has two steps: solving for the initial value and generalized line iteration solution.

A. Solving for the Initial Value

The 2-D affine LBTM is expressed as

$$\begin{aligned} a_{xT} &= C_1 + C_2 A_{xR} + C_3 A_{yR} \\ a_{yT} &= C_4 + C_5 A_{xR} + C_6 A_{yR} \end{aligned} \tag{1}$$

Manuscript received August 23, 2013; revised October 22, 2013 and November 16, 2013; accepted December 2, 2013. Date of publication January 10, 2014; date of current version March 11, 2014. This work was supported in part by the National Natural Science Foundation of China under Grant 41101407, Grant 41001260, and Grant 41101406; by the Ministry of Science and Technology of China under Project 2012BAJ15B04 and Project 2012AA12A305; by the Key Laboratory of Disaster Reduction and Emergency Response Engineering of the Ministry of Civil Affairs of China under Grant LDRERE20120206; and by the Natural Science Foundation of Hubei Province, China, under Grant 2010CDZ005.

C. Li is with the College of Urban and Environmental Sciences, Central China Normal University, Wuhan 430079, China, and also with the Key Laboratory of Disaster Reduction and Emergency Response Engineering, Ministry of Civil Affairs of China, Beijing 100124, China (e-mail: lcshaka@126.com; lichang@mail.ccnu.edu.cn).

W. Shi is with the Joint Spatial Information Research Laboratory, The Hong Kong Polytechnic University, Hong Kong, and also with Wuhan University, Wuhan 430079, China (e-mail: lswzshi@inet.polyu.edu.hk).

Color versions of one or more of the figures in this paper are available online at http://ieeexplore.ieee.org.

Digital Object Identifier 10.1109/LGRS.2013.2293844

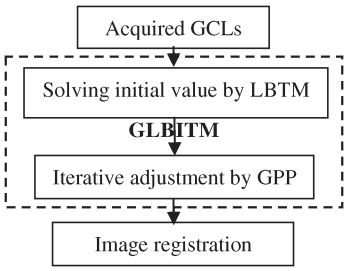

Fig. 1. Logic flow of image registration by the GLBITM.

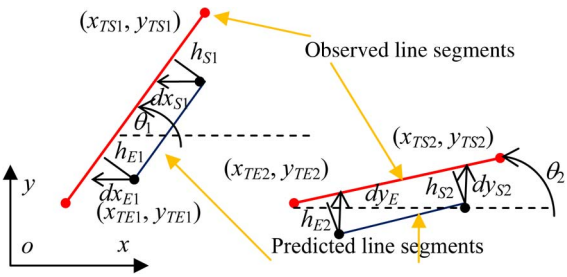

Fig. 2. Generalized line model. Error between the observed and predicted line segments.

where (a_{xT}, a_{yT}) are unit vector components of a line segment in the target image coordinate system, (A_{XR}, A_{YR}) are unit vector components of a corresponding line segment in the reference image coordinate system, and $C_1, \ldots, C_6$ are model coefficients. C_2, C_3, C_5, and C_6 are scale and rotation coefficients. C_1 and C_4 are translation coefficients.

The unit vector components in both target and reference image coordinate systems can be calculated from the two endpoints on a line segment by using

$$a_{xT} = \frac{x_{TE} - x_{TS}}{\sqrt{(x_{TE} - x_{TS})^2 + (y_{TE} - y_{TS})^2}}$$
$$a_{yT} = \frac{y_{TE} - y_{TS}}{\sqrt{(x_{TE} - x_{TS})^2 + (y_{TE} - y_{TS})^2}} \quad (2)$$
$$A_{xR} = \frac{X_{RE} - X_{RS}}{\sqrt{(X_{RE} - X_{RS})^2 + (Y_{RE} - Y_{RS})^2}}$$
$$A_{yR} = \frac{Y_{RE} - Y_{RS}}{\sqrt{(X_{RE} - X_{RS})^2 + (Y_{RE} - Y_{RS})^2}} \quad (3)$$

where (x_{TE}, y_{TE}), (x_{TS}, y_{TS}) are coordinates of the two endpoints on the line segment in the target image coordinate system. (X_{RE}, Y_{RE}), (X_{RS}, Y_{RS}) are the coordinates of the two endpoints on the line segment in the reference image coordinate system.

Notably, the unit vectors $(a_{xT}, a_{yT}, A_{XR}, A_{YR})$ do not provide a unique representation of two corresponding lines; the LBTM expresses the relationship between a group of lines. Therefore, the two endpoints defining the line segment unit vector in the target and reference images are not necessarily conjugate (corresponding) points, although the line segments they lie on must be conjugate lines.

After solving for coefficients $C_1, \ldots, C_6$, the initial values of $C_1, \ldots, C_6$ can be obtained. However, unit vectors in (1) do not provide a unique representation of a line, and as a result, the LBTM expresses the relationship between a group of lines in image space and any parallel group of lines in object space. Rotation and scale coefficients are good approximations, but translation coefficients usually display differences from the true value; this issue can be resolved by following the steps below.

B. Generalized Line Iteration

A significant difference between GPP and conventional point photogrammetry is that image features are not necessarily exact; this is also an advantage of the LBTM method. Because two endpoints of corresponding line segments are not necessarily conjugate points in both LBTM and GPP, the GPP methodology can be adopted to recalculate affine coefficients. In the generalized line model (see Fig. 2), the distance between observed and predicted line segments is divided into two components along the x- and y-axes of the image coordinate system. Using the initial values of coefficients $C_1, \ldots, C_6$, predicted line segments can be acquired by transforming line segments from the reference image to a target image. Instead of using the distance $(h_{S1}, h_{E1}, h_{S2}, h_{E2})$ from the endpoints of a predicted line segment to the endpoints of observed line segments as the error function, the differences dx_{S1}, dx_{E1}, dy_{S2}, and dy_{E2} between the endpoints of the predicted line segments and the observed line segments along the x- and y-axes are used as error functions. This works as long as the slope of the observed line segments is larger than 1.0 $(45^\circ \le |\theta| \le 90^\circ)$ or smaller than 1.0 $(0^\circ \le |\theta| < 45^\circ)$, respectively. This is because a vertical shift dy or a horizontal shift dx of the line segment makes a limited contribution to minimizing the disparity between the predicted and observed line segments. Notably, in the preceding definition of the error function, the greatest advantage is that exact conjugacy between two endpoints of corresponding line segments is not a prerequisite. Further explanation of this principle can be found in the literature [9].

Unlike the usual GPP method, the collinearity equation is not used in this method, and unlike the traditional LBTM method, which is an affine transformation model, the generalized line iteration that can be extended from a degree-1 to a degree-2 polynomial is calculated using (4), shown at the bottom of the page, where $C_1, \ldots, C_6$, (x_{TE}, y_{TE}), (x_{TS}, y_{TS}), (X_{RE}, Y_{RE}) and (X_{RS}, Y_{RS}) have the same meaning as in (1)–(3). $D_1, \ldots, D_6$ are quadratic coefficients; their values are generally small. Therefore, in the adjustment, the initial values can be given as $0, \ldots, 0$. $|\theta|$ is the absolute value of the angle

$$\left.\begin{aligned} x_{TE} &= C_1 + C_2 X_{RE} + C_3 Y_{RE} + D_1 X_{RE}^2 + D_2 X_{RE} Y_{RE} + D_3 Y_{RE}^2 \\ x_{TS} &= C_1 + C_2 X_{RS} + C_3 Y_{RS} + D_1 X_{RS}^2 + D_2 X_{RS} Y_{RS} + D_3 Y_{RS}^2 \end{aligned}\right\} \quad |\theta| \ge 45^\circ$$
$$\left.\begin{aligned} y_{TE} &= C_4 + C_5 X_{RE} + C_6 Y_{RE} + D_4 X_{RE}^2 + D_5 X_{RE} Y_{RE} + D_6 Y_{RE}^2 \\ y_{TS} &= C_4 + C_5 X_{RS} + C_6 Y_{RS} + D_4 X_{RS}^2 + D_5 X_{RS} Y_{RS} + D_6 Y_{RS}^2 \end{aligned}\right\} \quad |\theta| < 45^\circ \quad (4)$$

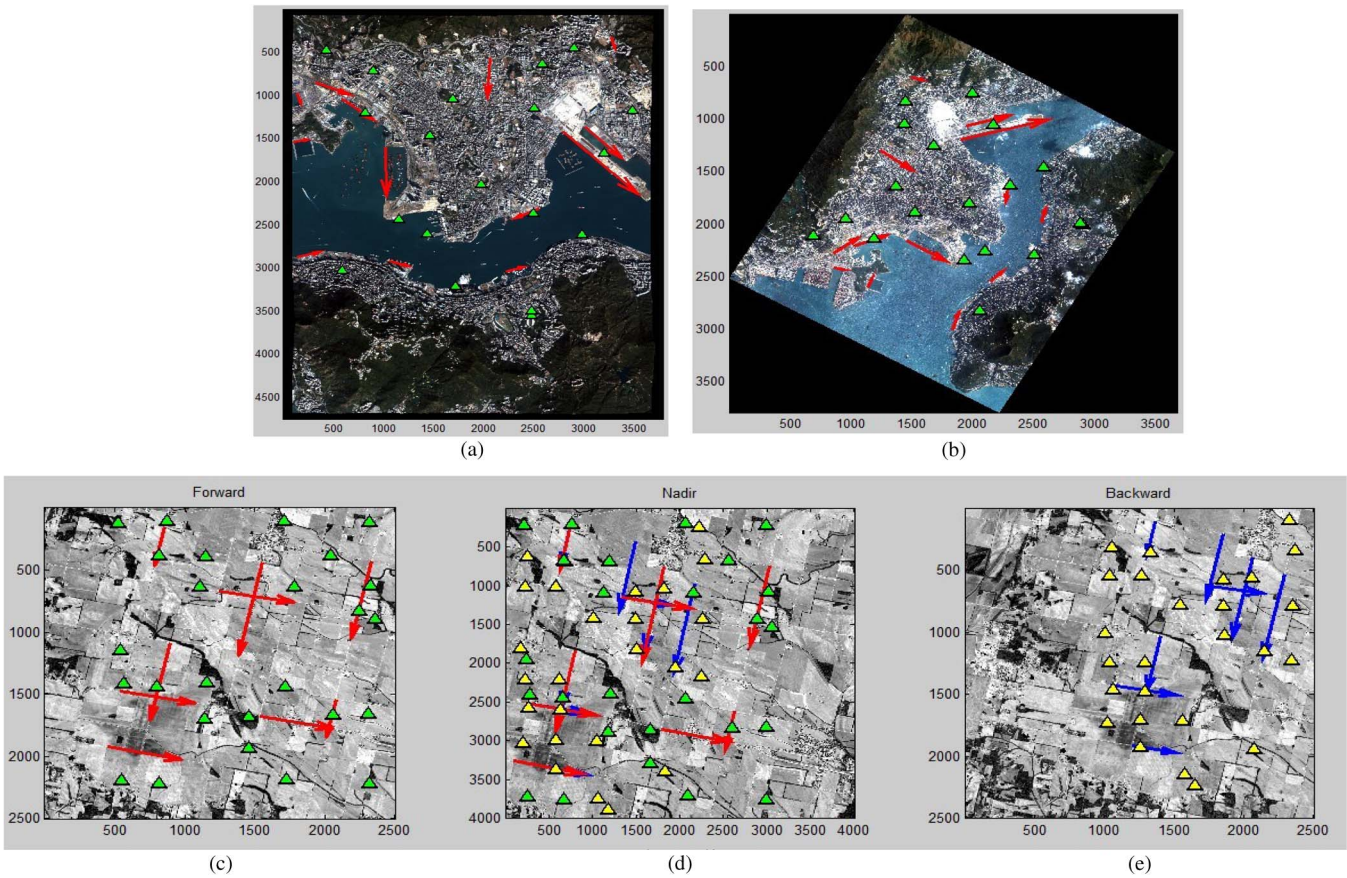

Fig. 3. Target image and reference image by manual digitizing. (a) Orthorectified QuickBird image. (b) IKONOS image with a manual rotation. (c) Forward. (d) Nadir. (e) Backward.

made with the x-axis ($0^\circ \le |\theta| \le 90^\circ$). Instead of using the traditional four equations, in this generalized line iteration, only two equations from (4) are used for an observed line segment with two endpoints. The error equations of the generalized line model with iterations are

$$\begin{aligned} v_x =& dC_1 + X_R \cdot dC_2 + Y_R \cdot dC_3 + X_{RE}^2 \cdot dD_1 \\ &+ X_{RE}Y_{RE} \cdot dD_2 + Y_{RE}^2 \cdot dD_3 - l_x \quad |\theta| \ge 45^\circ \\ v_y =& dC_4 + X_R \cdot dC_5 + Y_R \cdot dC_6 + X_{RE}^2 \cdot dD_4 \\ &+ X_{RE}Y_{RE} \cdot dD_5 + Y_{RE}^2 \cdot dD_6 - l_y \quad |\theta| < 45^\circ \end{aligned} \tag{5}$$

where $dC_1, \ldots, dC_6$ and $dD_1, \ldots, dD_6$ are the corrections to the coefficients $C_1, \ldots, C_6$ and $D_1, \ldots, D_6$, respectively. (X_R, Y_R) express (X_{RE}, Y_{RE}) and (X_{RS}, Y_{RS}). lx and ly are the aforementioned $-dx$ and $-dy$ values; these can be calculated by

$$\begin{aligned} l_x &= ((y) - y_{TS}) \cdot (x_{TE} - x_{TS}) \div (y_{TE} - y_{TS}) + x_{TS} - (x) \\ l_y &= ((x) - x_{TS}) \cdot (y_{TE} - y_{TS}) \div (x_{TE} - x_{TS}) + y_{TS} - (y) \end{aligned}$$

where (x) and (y) are the endpoint coordinates of predicted line segments and approximations. These are obtained from the results of the last iteration solving for $C_1, \ldots, C_6$ and $D_1, \ldots, D_6$. If the quadratic terms are ignored ($D_1 =, \ldots, = D_6 = 0$), then an affine transformation model can be also acquired.

Gross error should be taken into account to improve the generality and robustness of the GLBITM. Quality control based on posterior variance estimation (iteration method with variable weights) can be utilized for gross error detection. A statistical method for hypothesis testing is provided in [11]

$$T_i = \frac{\hat{\sigma}_i^2}{\hat{\sigma}_0^2} = \frac{v_i^2}{\hat{\sigma}_0^2 q_{v_{ii}} p_i} \sim F_\alpha(1, r) \quad (i = 1, 2, 3, \ldots, n) \tag{6}$$

where $\hat{\sigma}_i^2 = \boldsymbol{V}_i^T \boldsymbol{V}_i / r_i$, $r_i = \mathrm{tr}(\boldsymbol{Q}_{VV}\boldsymbol{P})_i$, $\hat{\sigma}_0^2 = \boldsymbol{V}^T\boldsymbol{P}\boldsymbol{V}/r = \boldsymbol{V}^T\boldsymbol{P}\boldsymbol{V}/(n-t)$, and T_i approximately obeys the F distribution with the degrees of freedom 1 and r. $\boldsymbol{Q}_{VV}\boldsymbol{P}$ is the reliability matrix, r is the degree of freedom, n is the observation number, and t is the essential observation number. The variable weight is then calculated by

$$p_i^{(v)} = \begin{cases} 1 & \text{when } T_i < F_{\alpha,1,r} \\ \frac{1}{T_i} & \text{when } T_i \ge F_{\alpha,1,r} \end{cases} \tag{7}$$

where $p^{(v)}$ is the weight at the vth time iteration.

III. Experiment and Discussion

Two image data sets taken at different times and by different sensors and different at oblique views were used to test the presented model.

1) The images chosen were the IKONOS (2000-11-27, 3678 pixels × 3801 pixels, GSD 4 m) and QuickBird (2004-01-25, 3790 pixels × 4760 pixels, GSD 2.4 m)

TABLE I
COMPARISON OF PBTM AND GLBITM

	C_1	C_2	C_3	C_4	C_5	C_6	Iters	GCPs (nums)	GCLs (nums)	ChkPs (nums)	RMSX (*pixel*)	RMSY (*pixel*)
PBTM1	314.803	0.310	0.513	2187.482	-0.514	0.310	—	26	—	19	**0.543**	**0.658**
GLBITM1	314.138	0.310	0.514	2187.140	-0.515	0.310	23	—	13	19	**0.515**	**0.571**
PBTM2	893.246	0.644	$-4.273*10^{-4}$	-53.891	0.001	0.588	—	20		26	**0.368**	**0.544**
GLBITM2	893.046	0.644	$-4.532*10^{-4}$	-54.018	0.002	0.588	16	—	10	26	**0.359**	**0.506**
PBTM3	382.257	0.646	$-3.144*10^{-4}$	-8.527	-0.002	0.592	—	20	—	27	**0.309**	**0.564**
GLBITM3	382.294	0.646	$-3.616*10^{-4}$	-8.519	-0.001	0.592	16	—	10	27	**0.299**	**0.543**

	C_1	C_2	C_3	C_4	C_5	C_6	D_1*10^{-7}	D_2*10^{-7}	D_3*10^{-7}	D_4*10^{-7}	D_5*10^{-7}	D_6*10^{-7}	Iters	RMSX (*pixel*)	RMSY (*pixel*)
PBTM1	316.963	0.309	0.506	2186.941	-0.514	0.309	3.9	-0.2	2.0	-0.5	1.7	0.2	—	**0.825**	**0.778**
GLBITM1	315.058	0.310	0.511	2187.428	-0.514	0.309	6.0	-2.4	3.6	-2.2	0.2	3.3	38	**0.602**	**0.697**
PBTM2	892.388	0.644	$2.373*10^{-4}$	-51.615	-3.030	0.586	-1.6	-1.7	-1.3	7.8	-0.4	4.2	—	**0.398**	**0.770**
GLBITM2	892.803	0.644	$-1.8*10^{-4}$	-52.007	$-5.787*10^{-4}$	0.587	1.4	-1.4	-0.003	7.7	0.7	3.5	16	**0.386**	**0.730**
PBTM3	382.521	0.645	$9.9*10^{-5}$	-9.303	$-6.1*10^{-4}$	0.592	1.1	2.0	-3.1	-2.4	-0.5	-0.1	—	**0.530**	**0.559**
GLBITM3	382.392	0.645	$5.4*10^{-4}$	-8.972	-0.001	0.592	1.1	1.4	-1.7	-1.0	-0.07	-0.9	16	**0.435**	**0.546**

images from Hong Kong (China). The QuickBird image was orthorectified as the reference image, and the IKONOS image was rotated to test the robustness of our model.

2) Ziyuan 3 or ZY-3 (in Chinese means Resources 3) is a Chinese Earth observation satellite launched in January 2012. ZY-3 is equipped with three-line scanners: panchromatic nadir (2.5 m), backward (4.0 m), and forward (4.0 m) views. The spatial subsets selected from the original images are the following: 4000 pixels × 4000 pixels, 2500 pixels × 2500 pixels, and 2500 pixels × 2500 pixels, respectively. In this experiment, the nadir was regarded as the reference image, and the other two (backward and forward) were regarded as target images. The view angle between the nadir and forward (or backward) images is 22°.

A number of corresponding line segments were digitized on the target and reference images; these were used as GCLs (see Fig. 3). Checkpoints were also selected for accuracy assessment (see Fig. 3). The coordinate system used in this experiment was an upper left corner coordinate system. In this system, the x and y coordinates map to pixels; values of x increase as the pixel moves right, and values of y increase as the pixel moves down.

The first step in the GLBITM is to solve for the initial values of $C_1, \ldots, C_6$. Then, by using (1)–(3), corresponding line segments are transformed from the reference image (QuickBird) coordinate system to the target image (IKONOS) coordinate system.

The second step of the GLBITM is to perform generalized line iteration by adjusting coefficients $C_1, \ldots, C_6$ and $D_1, \ldots, D_6$ to complete the final registration. The error equation (5) is used to quantify the difference between the observed and predicted line segments. The significance level α for hypothesis testing in (6) was set at 0.25 when applied to the iteration method with variable weights. When the unit weight mean square error $\hat{\sigma}_0$ was less than 10^{-4} or when the corrections $dC_1, \ldots, dC_6$ and $dD_1, \ldots, dD_6$ were all less than 10^{-6}, the iteration was halted.

Finally, the accuracy of the results obtained by applying the traditional point-based transformation model (PBTM) and the established GLBITM using both degree-1 and degree-2 polynomials are displayed in Table I.

Notably, the data set did not contain any steep slope GCL values. In addition, to guarantee comparability between the PBTM and the GLBITM, GCPs were selected on the GCLs to ensure consistency of ground control distribution; this is important for image rectification. In Table I, PBTM1 and GLBITM1 were the test results of data set 1. PBTM2 and GLBITM2 correspond to data set 2 (with the backward image regarded as the reference image). PBTM3 and GLBITM3 correspond to data set 2 (with the forward image regarded as the reference image). The coefficients of an affine and quadratic polynomial transformation are shown in Table I. Although there are initial translation errors of nearly $dx = 314$ pixels and $dy = 2187$ pixels in (C_1, C_4) after 23 iterations, the GLBITM did converge. There is a gradual change in $C_1, \ldots, C_6$ (iterations shown in Fig. 4), and we find that, after about the sixth iteration, the parameters tend to converge. Therefore, we conclude that this proposed approach is very robust. It is also important to note that the initial values of C_2, C_3, C_5, and C_6 for the rotation parameters provided by the LBTM were productive. The number of checking points (ChkPs) is shown for different data sets. The root-mean-square errors estimated by Chkps are shown in Table I. Subpixel accuracy is achieved by both PBTM and GLBITM. As shown in the RMSX and RMSY values in Table I, the accuracy of the authors' transformation model (GLBITM) is superior to the traditional PBTM when applied to different sensors, angles, and resolutions. To ensure the accuracy of the GLBITM, longer GCLs should be selected because they provide more reliable observations than shorter GCLs.

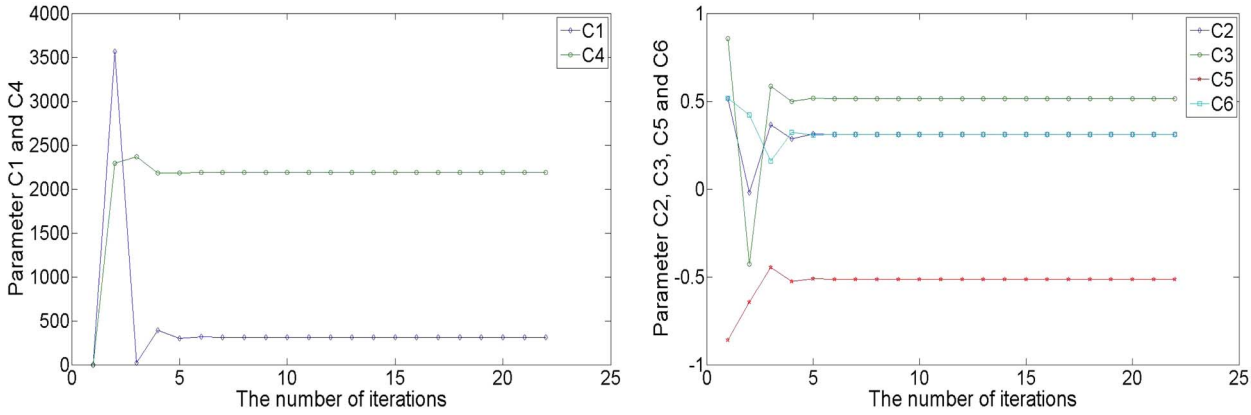

Fig. 4. Change of parameters $C_1, \ldots, C_6$ with the iterations in the experiment of data set 1.

In addition, the accuracy of the degree-2 polynomial is lower than that of the degree-1 polynomial. We also find that the values of $D_1, \ldots, D_6$ are very small (close to zero) in Table I. Although a second-order polynomial model is usually utilized in image registration, the higher order polynomial has an over-parameterization problem in practical applications. Thus, the GLBITM of a first-order model has a certain applied value.

IV. Conclusion

This letter has presented the GLBITM method, which can be used for image-to-image registration, rectification, and change detection. This is a GCL model without the use of any GCPs. The advantages of both LBTM and GPP are integrated within the GLBITM. That is, line segments do not have to be conjugate segments, although the straight lines on which they lie must be conjugate lines. The model has robust convergence when following the iteration method with variable weights and based on posterior variance estimation. The model can be applied to images captured by different sensors and resolution levels.

The GLBITM approach can potentially be widely used in many areas, such as remote sensing image processing and data updating, computer vision, machine vision, medical imaging, and military automatic target recognition.

Future research may be focused on automatic line segment matching to improve the automation level for image registration based on GLBITM. A confident registration with a given measure of uncertainty will be also studied in the future.

Acknowledgment

The authors would like to thank the anonymous reviewers and members of the editorial team for their comments and contributions.

References

[1] D. Boardman, "An automatic image registration system for SPOT data," *Int. Archives Photogramm. Remote Sens.*, vol. 31, pp. 128–133, 1996.
[2] L. G. Brown, "A survey of image registration techniques," *ACM Comput. Surveys (CSUR)*, vol. 24, no. 4, pp. 325–376, Dec. 1992.
[3] L. C. Chen and L. H. Lee, "Progressive generation of control frameworks for image registration," *Photogramm. Eng. Remote Sens.*, vol. 58, no. 9, pp. 1321–1328, Sep. 1992.
[4] J. Ton and A. K. Jain, "Registering Landsat images by point matching," *IEEE Trans. Geosci. Remote Sens.*, vol. 27, no. 5, pp. 642–651, Sep. 1989.
[5] A. F. Habib, H. T. Lin, and M. F. Morgan, "Line-based modified iterated Hough transform for autonomous single-photo resection," *Photogramm. Eng. Remote Sens.*, vol. 69, no. 12, pp. 1351–1358, 2003.
[6] W. Shi and A. Shaker, "The line-based transformation model (LBTM) for image-to-image registration of high-resolution satellite image data," *Int. J. Remote Sens.*, vol. 27, no. 14, pp. 3001–3012, Jul. 2006.
[7] A. F. Habib and R. I. Alruzouq, "Line-based modified iterated Hough transform for automatic registration of multisource imagery," *Photogramm. Rec.*, vol. 19, no. 105, pp. 5–21, Mar. 2004.
[8] Z. Zhang and J. Zhang, "Generalized point photogrammetry and its application," in *Proc. Int. Archives Photogramm. Remote Sens. Spatial Inf. Sci.*, Istanbul, Turkey, 2004, pp. 77–81.
[9] Z. Zhang, Y. Zhang, J. Zhang, and H. Zhang, "Photogrammetric modeling of linear features with generalized point photogrammetry," *Photogramm. Eng. Remote Sens.*, vol. 74, no. 9, pp. 1119–1127, Sep. 2008.
[10] C. Li, X. Li, C. Li, and Q. Li, "Application of generalized point photogrammetry to framework reconstruction of building facade," *Geomatics Inf. Sci. Wuhan Univ.*, vol. 36, no. 12, pp. 1451–1455, 2011.
[11] D. Li and X. Yuan, *Error Processing and Reliability Theory*. Wuhan, China: Publishing House Wuhan Univ., 2002.